RSC Advances

PAPER

View Article Online
View Journal | View Issue

Cite this: *RSC Adv.*, 2025, **15**, 48092

Computational design, synthesis, *in vitro* and *in vivo* evaluation of a 3,4-methylenedioxyphenol (sesamol) derivative as an NRF2/HO-1 pathway activator for protection against drug-induced liver injury

Ajay Mili,[a] Sumit Birangal,[b] Krishnadas Nandakumar,[c] Raghu Chandrashekar Hariharapura,[d] Nitesh Kumar,[e] Aravinda Pai[b] and Richard Lobo *[a]

Drug-induced liver injury is a major clinical and pharmacological challenge, often driven by oxidative stress and inflammation. This study aimed to develop a sesamol derivative with enhanced hepatoprotective efficacy *via* NRF2/HO-1 pathway activation. A focused virtual library of sesamol derivatives was generated through reaction-based enumeration and evaluated utilizing molecular docking and molecular dynamics simulations. Among 189 designed compounds, compound 133840-3CaBen (SMD) demonstrated superior binding to the KEAP1–NRF2 interface and was selected for synthesis and biological evaluation. *In vitro* antioxidant assays revealed that SMD exhibited a 4.5-fold lower IC_{50} compared to sesamol. In HepG2 cells, SMD conferred up to 62.99% protection against paracetamol-induced toxicity. *In vivo*, SMD (100 & 200 mg per kg b.w. orally) significantly restored liver enzyme profiles, and antioxidant markers (CAT, GSH, GPx, SOD) and reduced MDA levels. ELISA analysis confirmed NRF2, HO-1, and γ-GCS upregulation with a concomitant decrease in TNF-α and IL-6. Histopathological examination of H&E-stained liver sections corroborated these findings, showing preserved hepatic architecture with minimal necrosis, inflammation, and vacuolation, especially in the SMD group, comparable to silymarin. Collectively, our findings suggest that structural modification of sesamol into SMD confers hepatoprotection, likely through upregulation of NRF2/HO-1 pathway proteins. These findings highlight SMD as a promising lead compound for developing NRF2-targeted hepatoprotective agents.

Received 14th October 2025
Accepted 25th November 2025

DOI: 10.1039/d5ra07867a

rsc.li/rsc-advances

1. Introduction

Drug-induced liver injury (DILI) remains a considerable obstacle in both clinical practice and drug development, often leading to treatment discontinuation or drug withdrawal from the market.[1,2] Its unpredictable nature and complex etiology render it a predominant factor in acute liver failure across numerous nations, contributing to high morbidity and healthcare costs.[3] The liver, being the primary site for the metabolism of xenobiotics, remains highly vulnerable to chemical insults, especially during the biotransformation of drugs into reactive intermediates.

Several interconnected mechanisms contribute to DILI, including mitochondrial dysfunction, immune-mediated responses, and disturbances in bile acid homeostasis. Among these, oxidative stress is regarded as a central player in the initiation and progression of liver injury.[4] Elevated levels of reactive oxygen species (ROS) can overwhelm the capacity of the intrinsic antioxidant mechanism, resulting in lipid peroxidation and DNA damage. These molecular alterations compromise hepatocyte viability and result in either apoptosis or necrosis, depending on the context and severity of the insult.[5]

To mitigate oxidative damage, mammalian cells have evolved multiple defense mechanisms, most notably through the activation of the nuclear factor erythroid 2-related factor 2 (NRF2) pathway. It functions as a redox-responsive transcription factor that coordinates the activation of multiple genes involved in cellular defense against oxidative stress, including

[a]*Department of Pharmacognosy, Manipal College of Pharmaceutical Sciences, Manipal Academy of Higher Education, Manipal, Karnataka-576104, India*
[b]*Department of Pharmaceutical Chemistry, Manipal College of Pharmaceutical Sciences, Manipal Academy of Higher Education, Manipal, Karnataka-576104, India*
[c]*Department of Pharmacology, Manipal College of Pharmaceutical Sciences, Manipal Academy of Higher Education, Manipal, Karnataka-576104, India*
[d]*Department of Pharmaceutical Biotechnology, Manipal College of Pharmaceutical Sciences, Manipal Academy of Higher Education, Manipal, Karnataka-576104, India*
[e]*Department of Pharmacology and Toxicology, National Institute of Pharmaceutical Education and Research (NIPER), Hajipur, Bihar-844102, India*

detoxification and anti-inflammatory pathways.[6] Under normal conditions, the NRF2 remains bound with Kelch-like ECH-associated protein 1 (Keap1) in the cytoplasm, which facilitates its ubiquitin-dependent degradation. However, during oxidative or electrophilic stress, alterations to specific cysteine residues on Keap1 impair this degradation process, enabling NRF2 to accumulate and move into the nucleus. Inside the nucleus, the unbounded NRF2 interacts with antioxidant response element (ARE) to stimulate the transcription of a wide array of genes, such as heme oxygenase-1 (HO-1), NAD(P)H:quinone oxidoreductase 1 (NQO1), glutamate–cysteine ligase catalytic subunit (GCLC), and various phase II detoxifying enzymes.[2,7]

Among these, the NRF2/HO-1 axis is particularly important for protecting the liver from oxidative injury. HO-1 enzymatically converts heme into biliverdin, carbon monoxide, and Fe^{2+}. Each of these by-products contributes in some way to cytoprotection, either through antioxidant, anti-inflammatory, or anti-apoptotic effects.[8] Therefore, pharmacologically targeting NRF2 to upregulate this defensive pathway is widely regarded as a viable approach to managing DILI and related hepatic disorders.[9]

However, while the therapeutic rationale is strong, progress in developing clinically viable NRF2 activators has been limited. Some synthetic activators have entered trials, but issues such as off-target effects, poor bioavailability, and long-term safety concerns have constrained their use.[10] These limitations have prompted a growing interest in natural products as alternative or complementary NRF2 modulators.

One such promising compound is sesamol (3,4-methylenedioxyphenol), a phenolic antioxidant found in sesame seeds (*Sesamum indicum* L).[11] It possesses a range of biological properties, including hepatoprotection,[12] anticancer,[13] upregulation of antioxidant enzymes,[14] ROS scavenging,[11] anti-inflammatory,[15] and cardioprotection[16] activities. Structurally, sesamol features a benzodioxole moiety and a hydroxyl group, both of which contribute to its strong radical-scavenging capacity. The presence of the dioxole ring enhances molecular rigidity and stability, while the phenolic hydroxyl facilitates electron donation, making it especially effective against ROS.[17,18] Despite these advantages, its clinical application remains limited. Issues such as accelerated metabolism, a short elimination half-life, suboptimal bioavailability *via* the oral route, and only moderate efficacy under intense oxidative stress have limited its therapeutic potential.[19,20] Although sesamol derivatives are known in chemical databases and patents, their biological activity as NRF2/HO-1 activators and hepatoprotective agents has not been reported. Our design rationale was to introduce a carboxymethyl linker followed by amide coupling with a benzoic acid derivative, thereby enhancing polarity and hydrogen-bonding potential compared to sesamol. This modification was hypothesized to improve KEAP1 binding affinity and stability, as supported by structure–activity considerations of phenolic antioxidants. In the present study, we generated a focused virtual library of sesamol derivatives using a reaction-based enumeration strategy with amines available in our laboratory. The designed compounds were evaluated for their ability to interact with the Keap1–NRF2 complex through molecular docking, MM-GBSA, and molecular-dynamics simulations. The top-scoring derivative was synthesized and subjected to *in vitro* and *in vivo* evaluation for antioxidant and hepatoprotective efficacy in a paracetamol-induced liver injury model. While the biological experiments primarily assessed NRF2 pathway activation, the computational analyses indicated favorable interactions of the compound within the KEAP1 pocket that binds NRF2, providing a plausible structural rationale for the observed activation.

This integrative computational-to-biological workflow was thus designed to identify a sesamol-based NRF2 activator with improved stability and hepatoprotective potential compared to the parent compound.

2. Result and discussion

An *O*-alkylation reaction was carried out between sesamol and chloroacetic acid under basic conditions, leading to the formation of 2-(benzo[*d*][1,3]dioxol-5-yloxy)acetic acid (**i**).[21] Through this reaction, a carboxymethyl group (–CH_2–COOH) becomes attached to the hydroxyl site on the sesamol molecule, thus introducing a functional handle for further modifications (Scheme 1). The newly introduced carboxyl functionality enables smooth coupling with a variety of aniline derivatives, allowing for the generation of structurally diverse sesamol-based compounds. This transformation is crucial as it converts the less reactive native sesamol into a more chemically versatile scaffold, paving the way for designing additional compounds.

2.1 Computational studies

2.1.1 Enumeration-based drug design, molecular docking, and MM-GBSA. A total of 189 sesamol derivatives were designed using the reaction-based enumeration module in Schrödinger and prepared using LigPrep at pH 7.4 (Fig. 1).

The designed ligands were docked into the KEAP1 protein (PDB ID: 4L7D), and their binding affinities were evaluated using the Glide XP and MM-GBSA methods. Based on their scoring profiles (docking: −6.32 to −9.34 kcal mol^{-1}; MM-GBSA: −55.08 to −80.31 kcal mol^{-1}), the ten top-scoring compounds were selected for detailed analysis.

The co-crystallized ligand (1VX) formed stabilizing interactions with key residues of KEAP1, including hydrogen bonds with SER602, ARG415, and ASN414, a hydrogen-bonded water bridge involving ASN382 and SER363, a salt bridge with ARG380, and a π–π interaction with TYR572. These interactions validated the reliability of the docking protocol and served as a reference for evaluating the designed sesamol derivatives.

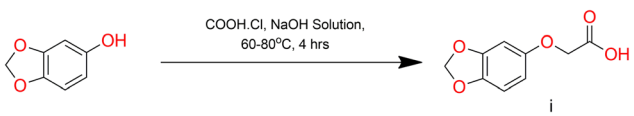

Scheme 1 Synthesis of 2-(benzo[d][1,3]dioxol-5-yloxy)acetic acid (**i**).

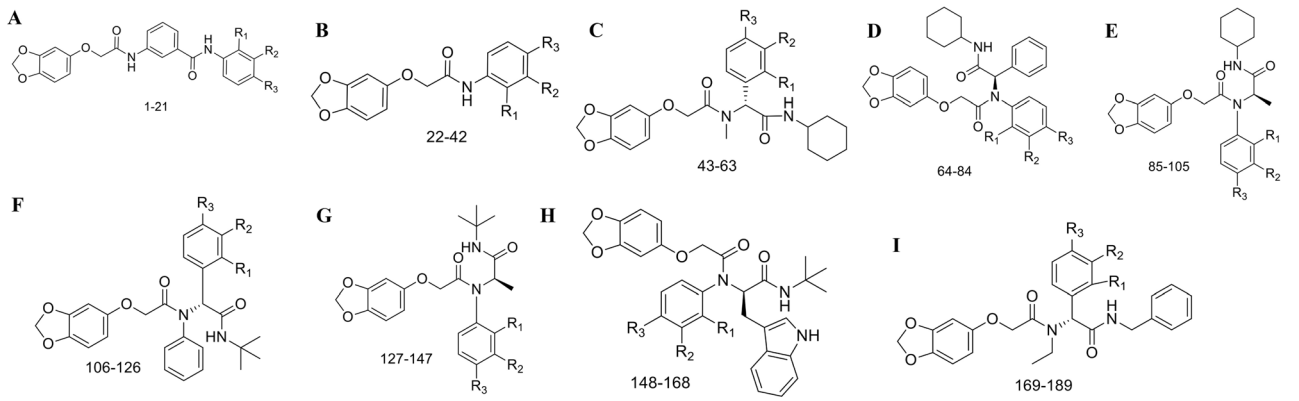

Sl. no	Title	R_1	R_2	R_3	Sl. no	Title	R_1	R_2	R_3
1	-2CF3Ben	CHF_3	H	H	12	-3MeBen	H	CH_3	H
2	-2ClBen	Cl	H	H	13	-Ben	H	H	H
3	-2FBen	F	H	H	14	-3OMeBen	H	OCH_3	H
4	-2HyBen	OH	H	H	15	-4CF3Ben	H	H	CHF_3
5	-2MeBen	CH_3	H	H	16	-4CaBen	H	H	COOH
6	-2OMeBen	OCH_3	H	H	17	-4ClBen	H	H	Cl
7	-3CF3Ben	H	CHF_3	H	18	-4FBen	H	H	F
8	-3CaBen	H	COOH	H	19	-4HyBen	H	H	OH
9	-3ClBen	H	Cl	H	20	-4MeBen	H	H	CH_3
10	-3FBen	H	F	H	21	-4OMeBen	H	H	OCH_3
11	-3HyBen	H	OH	H					

Fig. 1 Compound title and R-group of the series, (A) 133699, (B) 133840, (C) 133861, (D) 133862, (E) 133863, (F) 133864, (G) 133865, (H) 133866, and (I) 133999.

Among the newly generated compounds, several derivatives demonstrated comparable or enhanced binding affinities relative to the co-crystallized ligand. 133699-2ClBen exhibited a favorable docking score (-7.42 kcal mol^{-1}) and MM-GBSA binding energy (-80.31 kcal mol^{-1}), forming hydrogen bonds with ASN382, ARG415, and SER602, along with a π–π interaction with TYR334. 133699-3OmeBen also maintained strong contacts with SER602 and ARG415 through hydrogen bonding and cation–π interactions, supported by π–π stacking with TYR334. The hydroxyl-substituted analogue 133699-3HyBen displayed the most favorable docking score (-9.34 kcal mol^{-1}), forming multiple hydrogen bonds with SER363, ARG380, ARG415, GLN530, and SER555, in addition to π–π and cation–π interactions with TYR334 and ARG415, respectively. Such an extensive network of polar and aromatic interactions suggested strong anchoring within the KEAP1 pocket. Similarly, 133699-4HyBen showed hydrogen bonding with SER363, ASN414, ARG415, SER508, and GLN530, accompanied by π–π stacking with TYR334, indicating a stable binding orientation. The derivative 133840-3HyBen established hydrogen bonds with SER363, ASN382, ASN414, and SER602, and maintained a cation–π interaction with ARG415, consistent with a favorable docking score (-6.32 kcal mol^{-1}). The compound 133840-4HyBen, which later emerged as the most promising hit, exhibited an extensive hydrogen-bonding network involving SER363, ASN382, ASN414, ARG415, and SER602, along with π–π stacking with TYR572 and a cation–π interaction with ARG415. These interactions indicate strong complementarity within the KEAP1 binding site. 133840-3CaBen also mirrored several interactions observed with the co-crystallized ligand, forming hydrogen bonds with ARG382, ASN414, and SER602, a water-mediated bridge *via* SER363 and ASN414, and a salt bridge with ARG415, reinforcing its potential stability. Among the halogenated derivatives, 133861-3ClBen (-7.12 kcal mol^{-1}) and 133862-2ClBen (-7.34 kcal mol^{-1}) exhibited π–π stacking with TYR572 and TYR334, respectively, as well as salt and cation–π interactions with ARG415, suggesting moderate binding strength. 133861-4HyBen formed hydrogen bonds with SER363, ARG415, and SER602, further stabilized by a cation–π interaction with ARG415, indicating a balanced electrostatic contribution to its binding energy. Overall, the docking and MM-GBSA analyses revealed that the designed sesamol derivatives effectively occupy the KEAP1 binding cavity through a conserved hydrogen-bonding network centered on ARG415, SER602, and ASN414.

The compound structures, docking scores, MM-GBSA values, and ligand–protein interactions of the top 10 compounds are summarized in Table 1, while their 2D interaction diagrams are provided in the SI (Fig. S1).

2.1.2 Absorption, distribution, metabolism & excretion (ADME) and drug likeness. In drug design, assessing drug-likeness and ADME properties is critical. Drug-likeness was evaluated using Lipinski's rule of five, where most compounds met these criteria without violations, except for 133862-2ClBen which violated one parameter. Oral absorption is another key factor, with eight compounds (133699-2ClBen, 133699-3HyBen,

Table 1 Title, structure, docking score, MM-GBSA, and interaction with protein of the top 10 compound

Title	Structure	Docking score (kcal mol^{-1})	MM-GBSA (kcal mol^{-1})	Interaction with protein
1VX	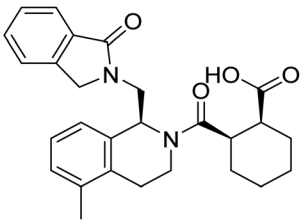	−7.038	−86.39	H-bond: SER602, ARG415, ASN414 H-bonded water bridge: ASN382, SER363 Salt bridge: ARG380 π–π interaction: TYR572
133699-2ClBen	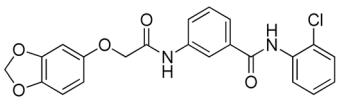	−7.42	−80.31	H-bond: ASN382, ARG415, SER602 π–π interaction: TYR334
133699-3OmeBen	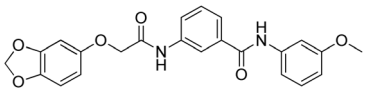	−6.8	−72.97	H-bond: SER602 π–π interaction: TYR334 Cation–π interaction: ARG415
133699-3HyBen	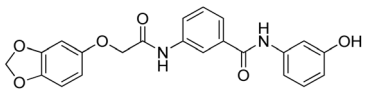	−9.34	−75.12	H-bond: SER363, ARG380, ARG415, GLN530, SER555 π–π interaction: TYR334 Cation–π interaction: ARG415
133699-4HyBen	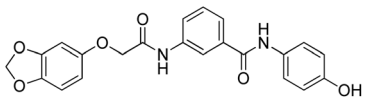	−7.19	−65	H-bond: SER363, ASN414, ARG415, SER508, GLN530 π–π interaction: TYR334
133840-3HyBen	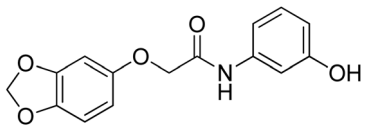	−6.32	−55.62	H-bond: SER363, ASN382, ASN414, SER602 Cation–π interaction: ARG415
133840-4HyBen	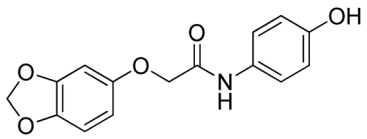	−7.18	−55.08	H-bond: SER363, ASN382, ASN414, ARG415, SER602 π–π interaction: TYR572 Cation–π interaction: ARG415
133840-3CaBen	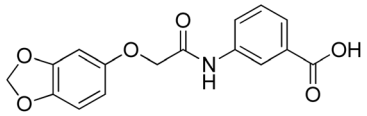	−7.2	−55.69	H-bond: ARG382, ASN414, SER602 H-bonded water bridge: SER363, ASN414 Salt bridge: ARG415
133861-3ClBen	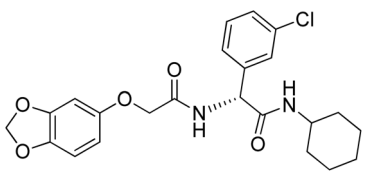	−7.12	−74.24	H-bond: ARG415, TYR572, SER602 π–π interaction: TYR572
133861-4HyBen	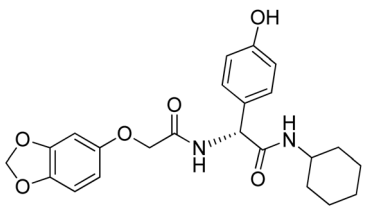	−7.87	−68.97	H-bond: SER363, ARG415, SER602 Cation–π interaction: ARG415

Table 1 (*Contd.*)

Title	Structure	Docking score (kcal mol^{-1})	MM-GBSA (kcal mol^{-1})	Interaction with protein
133862-2ClBen	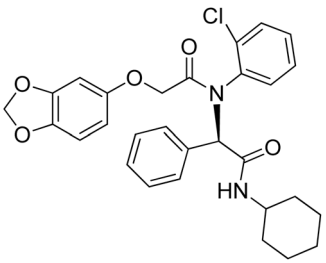	−7.34	−77.19	Salt bridge: ARG415 π–π interaction: TYR334, TYR572 Cation–π interaction: ARG415

133699-3OMeBen, 133699-4HyBen, 133840-3HyBen, 133840-4HyBen, 133861-3ClBen, 133862-2ClBen) exhibiting absorption rates of 90% or higher. In contrast, 133840-3CaBen and 133861-4HyBen shows absorption of 72% and 8%, respectively. Hydrogen bond donors and acceptors were evaluated against the acceptable ranges of 0.0 to 6.0 and 2.0 to 20.0, respectively, with all compounds falling within these limits. Additionally, predicted pharmacokinetic parameters were within the recommended thresholds: QPlogS values ranged from −5.38 to −2.27 (within −6.5 to 0.05), QPlogKhsa values ranged from −0.514 to 0.392 (within −1.5 to 1.5), and QPlogBB values ranged from −5.38 to −2.27 (within −3 to 1.2) (SI Table S1).

2.1.3 Molecular dynamic simulation (MDS) studies. In MDS studies, convergence was evaluated using several key parameters. The root mean square deviation (RMSD) and root mean square fluctuation (RMSF) were monitored to assess structural stability and atomic movement consistency, respectively. Complex total energy was tracked to ensure equilibrium, while Principal Component Analysis (PCA) and the Free Energy Landscape (FEL) evaluated motion stability and energy distribution. The radius of gyration (rGyr) assessed molecular compactness, solvent-accessible surface area (SASA), and post MD-MM/GBSA calculations estimated binding free energy analysis confirmed solvent exposure stability. Based on docking score, ADME properties, drug-likeness, and MM-GBSA results, 10 compounds (133699-2ClBen, 133699-3HyBen, 133699-3OMeBen, 133699-4HyBen, 133840-3HyBen, 133840-4HyBen, 133840-3CaBen, 133861-3ClBen, 133861-4HyBen, and 133862-2ClBen) were selected for MDS over a 50 ns simulation period. Following this screening, compound 133840-3CaBen was chosen for an extended 500 ns simulation and discussed below. Interestingly, literature search revealed that this compound had been previously synthesized and reported in the chemical literature.[22] However, its biological activity, particularly its potential to activate NRF2 and protect against DILI, has not been described. This finding provided an opportunity to evaluate a known chemical entity in a novel biological context. Ligand–protein complexes were generated, with complex-**1** representing the KEAP1–co-crystallized ligand complex and complex-**2** representing the KEAP1–133840-3CaBen complex.

2.1.3.1 Protein–ligand complex RMSD and RMSF. The Prot Cα RMSD of complex-**1** and complex-**2** ranged from 0.696 Å to 1.41 Å and 0.699 Å to 1.356 Å, with average values of 0.99 Å and 0.98 Å, respectively (Fig. 2A). Similarly, the Lig fit Prot RMSD ranged from 0.29 Å to 1.37 Å for complex-**1** and 0.44 Å to 2.29 Å for complex-**2**, with average values of 0.69 Å and 1.21 Å (Fig. 2B). Throughout the 500 ns simulation, both Prot RMSD and Lig fit Prot RMSD values remained relatively stable, indicating minimal conformational changes and suggesting that both complexes maintained structural integrity and consistent protein–ligand interactions over the simulation period.

The RMSF values (in Å) for key residues in complex-**1**—TYR334, SER363, ASN382, ASN414, ARG415, TYR525, ALA556, TYR572, PHE577, and SER602—were 0.396, 0.344, 0.550, 0.304, 0.303, 0.454, 0.369, 0.398, 0.440, and 0.381, respectively. Corresponding values for complex-**2** were 0.415, 0.366, 0.639, 0.334, 0.325, 0.450, 0.427, 0.450, 0.414, and 0.378 Å, respectively (Fig. 2C). The overall fluctuation patterns of complex-**2** were consistent with those of complex-**1**, suggesting that the compound (133840-3CaBen) maintained a binding profile similar to the co-crystallized ligand. This similarity underscores the structural stability of key residues and indicates that the test compound established interactions comparable to those of the co-crystallized ligand. The protein–ligand complex interaction, protein–ligand contact timeline, and interaction images are shown in the SI (Fig. S2).

2.1.3.2 PCA, post MD MMGBSA dG bind, and FEL. PCA analysis revealed that complexes (**1** & **2**) share a dense central cluster, indicating partial conformational similarity. However, the broader dispersion observed in complex-**2**, particularly along PC1 and PC2, suggests increased conformational flexibility. These findings suggest that although complex-**2** adopts some conformations similar to those of complex-**1**, it also samples a broader conformational space, indicative of decreased structural stability (Fig. 3A).

The post-MD binding free energy for complex-**1** and complex-**2** ranged from −58.52 to −78.90 kcal mol^{-1} and

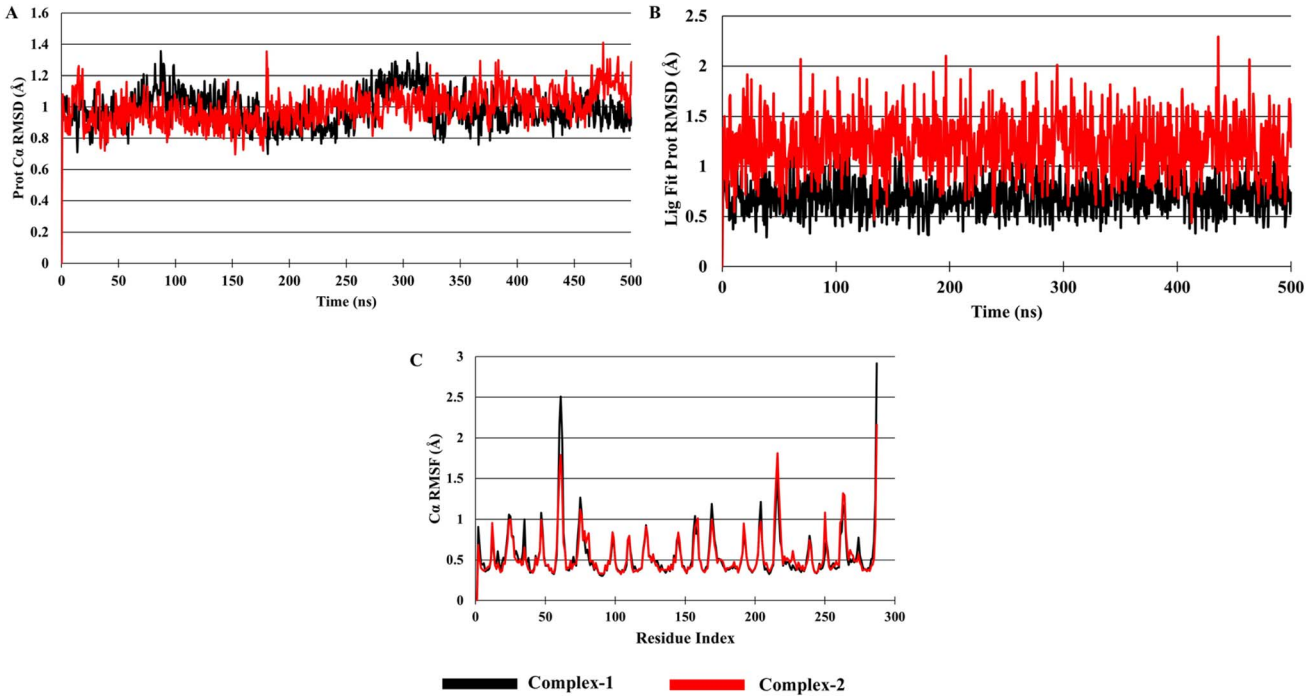

Fig. 2 (A) Ligand protein complex RMSD, (B) Lig fit Prot RMSD, and (C) ligand–protein complex RMSF.

−38.16 to −64.00 kcal mol^{-1}, respectively, with average values of −66.65 kcal mol^{-1} and −50.74 kcal mol^{-1} (Fig. 3B). The lower value observed for complex-**1** indicates a stronger binding affinity of the co-crystallized ligand compared to the test compound. However, the bind of complex-**2** remained within a favorable range, suggesting that the test compound maintained substantial binding interactions with the target protein, potentially contributing to complex stability throughout the simulation.

The PCA-based FEL revealed notable differences in the conformational stability between complex-**1** and complex-**2**. In complex-**1**, multiple well-defined low-energy basins indicate a high degree of conformational flexibility and a less stable structural state (Fig. 3C). In contrast, complex-**2** exhibited a single dominant energy minimum, suggesting a more restricted conformational space and greater structural rigidity (Fig. 3D). This reflects enhanced conformational stability, implying that complex-**2** forms a more stable and tightly bound structure compared to complex-**1**.

2.1.3.3 SASA, radius of gyration rGyr, and TE. The rGyr for complex-**1** varied from 4.19 Å to 4.47 Å, with a mean value of 4.33 Å, while for complex-**2**, it ranged from 3.65 Å to 4.64 Å, averaging 4.27 Å (Fig. 4A). The comparable rGyr values between the two complexes indicate minimal structural deviations, suggesting that both the co-crystallized ligand and test compound maintained overall structural compactness and stability throughout the simulation.

The SASA of complex-**1** ranged from 123.30 Å^2 to 217.74 Å^2, with an average value of 172.61 Å^2, whereas complex-**2** exhibited a SASA range of 91.12 Å^2 to 199.73 Å^2, averaging 163.29 Å^2 (Fig. 4B). The slightly lower SASA of complex-**2** suggests a more compact conformation compared to complex-**1**, potentially indicating tighter packing or reduced solvent exposure of the test compound.

The TE of complex-**1** ranged from 350252.72 to 351289.38 kcal mol^{-1}, with an average of 350775.45 kcal mol^{-1}, while complex-**2** exhibited a TE range of 350771.91 to 351881.03 kcal mol^{-1}, with an average of 351265.59 kcal mol^{-1}. The slightly higher total energy of complex-**2** suggests that the test compound may induce marginally greater conformational adjustments compared to the co-crystallized ligand, potentially due to differences in binding interactions or steric effects. Both complexes exhibited similar energy trends, reflecting their stable structures throughout the course of the simulation.

2.2 Chemistry

Based on molecular docking and MDS studies, the compound 133840-3CaBen was identified as a potential candidate and subsequently synthesized. The IUPAC name of the compound is 3-(2-(benzo[*d*][1,3]dioxol-5-yloxy)acetamido)benzoic acid (SMD), and its synthesis is outlined in Scheme 2.

The synthesis began with the preparation of the ester intermediate, ethyl 3-(2-(benzo[*d*][1,3]dioxol-5-yloxy)acetamido) benzoate (**ii**), which was subsequently hydrolyzed to the corresponding carboxylic acid, 3-(2-(benzo[*d*][1,3]dioxol-5-yloxy) acetamido)benzoic acid (**iii**), under basic conditions using NaOH. This transformation was implemented to increase polarity and potential binding interactions. The hydrolysis proceeded smoothly, yielding the desired carboxylic acid.

The structure of the compound was confirmed by FTIR, LC-MS, ^{1}H NMR, and ^{13}C NMR analysis.

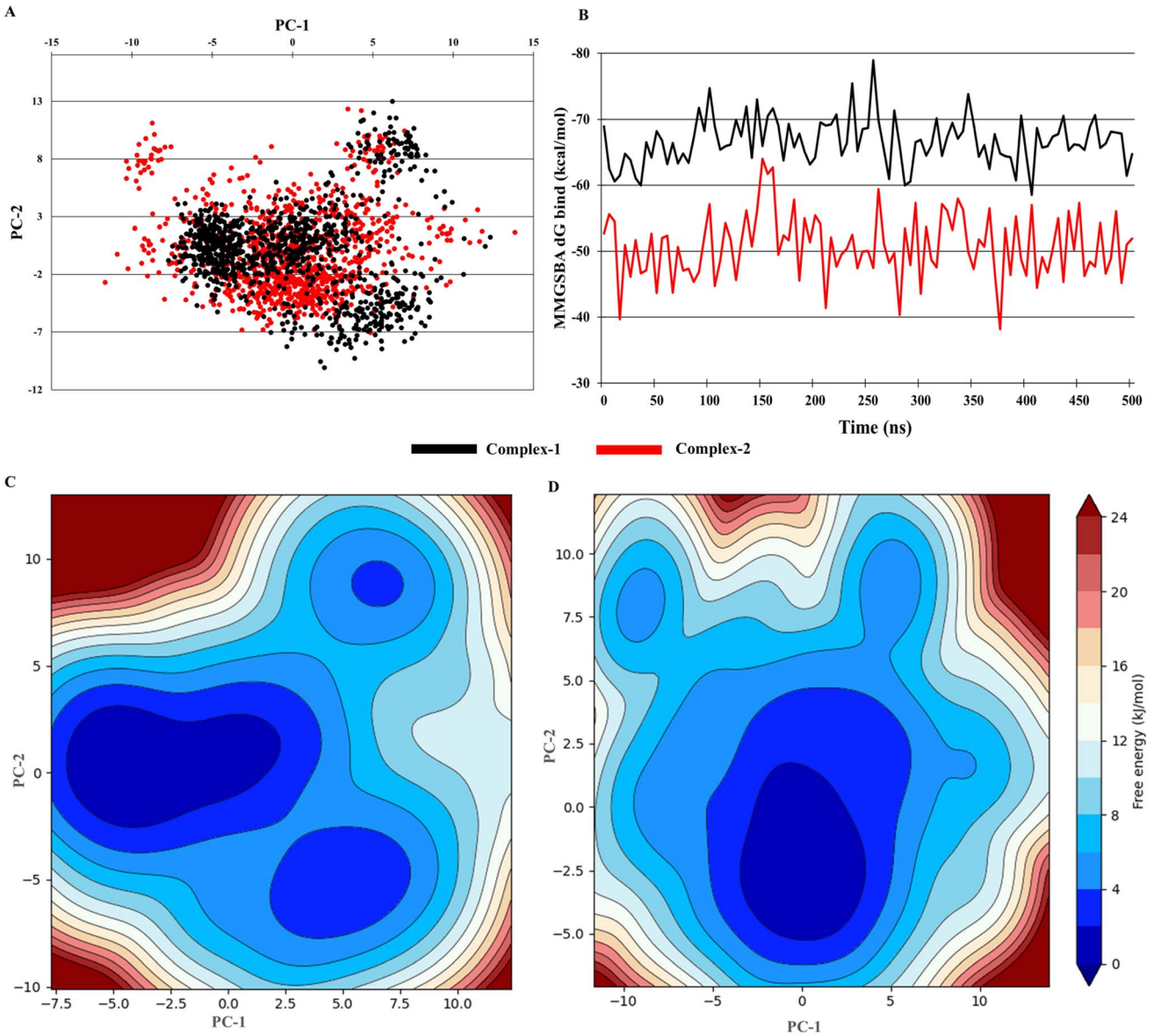

Fig. 3 (A) Scatter plot of PC-1 *vs.* PC-2 of the complexes, (B) post-MD binding free energy of the complexes, (C) free energy landscape of complex-**1**, and (D) free energy landscape of complex-**2**.

2.3 *In vitro* antioxidant, cytotoxicity, and protective activity against paracetamol (PCM)-induced toxicity assay

2.3.1 Antioxidant assay. The antioxidant potential of SMD and sesamol (SM) was evaluated using the DPPH assay, with ascorbic acid as the standard reference. The structural modification in SMD resulted in a notable increase in radical scavenging capacity, as reflected by a significantly lower IC_{50} value of 32.79 μg mL^{-1} compared to 148.86 μg mL^{-1} for SM, indicating a nearly 4.5-fold enhancement in efficacy (Fig. 5). The improved antioxidant activity of SMD may be attributed to its structural features that potentially enhance electron donation, thereby stabilizing free radicals more effectively. Thus, SMD emerges as a promising antioxidant agent with superior efficacy relative to its parent compound, SM.

2.3.2 Cell cytotoxicity and protective activity against PCM-induced toxicity in HepG2 cell line. Cell cytotoxic effects of SM and SMD, six concentrations ranging from 31.25 to 1000 μg mL^{-1} were employed. The IC_{50} value for SM was determined to be 536.41 μg mL^{-1}, whereas SMD displayed a peak inhibitory effect of 44% at the maximum tested concentration of 1000 μg mL^{-1} (Fig. 6A).

Based on the cytotoxicity analysis, concentrations ranging from 6.25 to 100 μg mL^{-1} were selected to evaluate the protective effects of SM and its derivative, SMD, against paracetamol (6 mM)-induced toxicity in HepG2 cells. Silymarin, a well-established hepatoprotective agent, was included as a standard and tested under identical conditions. HepG2 cells were pretreated with the test compounds for 24 hours, followed by a 48 hour exposure to Paracetamol. SMD shows protective

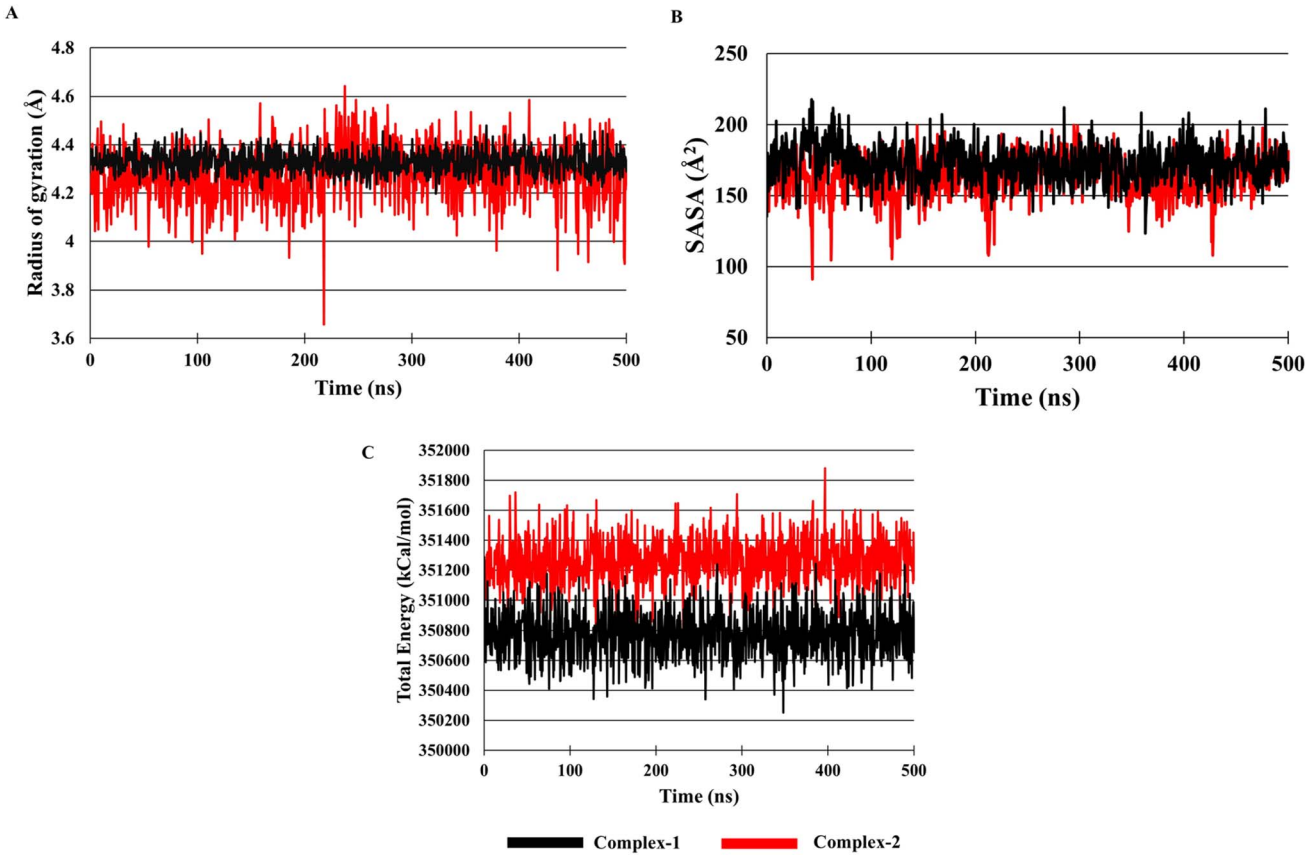

Fig. 4 (A) Radius of gyration of the complexes, (B) SASA of the complexes, and (C) total energy of the complexes.

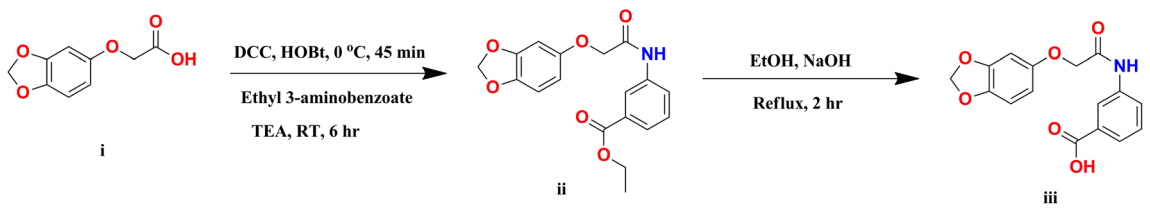

Scheme 2 Synthesis of 3-(2-(benzo[*d*][1,3]dioxol-5-yloxy)acetamido)benzoic acid (SMD).

activity, achieving a maximum of 62.99% protection at 12.5 μg mL^{-1} and maintaining significant protection at 25 μg mL^{-1} with 58.92% cell viability as compared to the paracetamol-induced toxicity group, which is significantly higher than SM, which reached peak protection of 55.31% at 6.25 μg mL^{-1}. SMD consistently maintained elevated protection across all tested concentrations, with mean cell viability values ranging from 41.66 ± 0.46% at 100 μg mL^{-1} to 62.99 ± 0.51% at 12.5 μg mL^{-1}, highlighting its potential as a more potent sesamol derivative (Fig. 6B).

2.4 *In vivo* evaluation of hepatoprotective potential

2.4.1 Biochemical studies. Serum biochemical analysis revealed significant hepatocellular injury in the PCM group, which is evident by elevated levels of aspartate aminotransferase (AST) ($P < 0.0001$), alanine aminotransferase (ALT) ($P < 0.001$), alkaline phosphatase (ALP) ($P < 0.0001$), and total bilirubin ($P < 0.001$) compared to the normal group, indicating hepatocellular damage and reduced clearance of bilirubin due to oxidative stress, necrosis, and inflammation. Treatment with silymarin significantly reduced these markers, confirming its hepatoprotective efficacy. Sesamol (SM-H and SM-L) showed a moderate reduction in enzyme levels. Interestingly, the sesamol derivative SMD, particularly at the high dose (SMD-H, 200 mg per kg b.w.), demonstrated a comparable hepatoprotective effect to silymarin (Fig. 7). These findings support the therapeutic potential of SMD as a promising alternative to silymarin. Furthermore, no statistically significant variation was detected in the levels of direct bilirubin, albumin, and total protein across all groups, suggesting intact synthetic and excretory functions even in the acute phase.

2.4.2 Evaluation of hepatic antioxidant status. The levels of catalase (CAT), glutathione (GSH), glutathione peroxidase

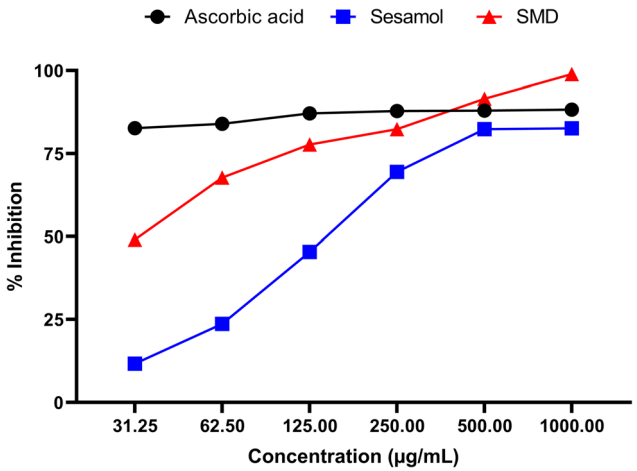

Fig. 5 DPPH radical scavenging activity of SMD, sesamol, and ascorbic acid. Each value represents mean ± SD.

(GPx), and sodium dismutase (SOD) of the liver homogenate have been significantly ($P < 0.0001$) reduced in the PCM group *vs.* control group, indicating severe depletion of the antioxidant defense system resulting in its inability to reduce ROS. Meanwhile, a significant increase ($P < 0.0001$) in the MDA levels of the control group was observed, an indicator of oxidative stress and damage to cellular membranes. Silymarin restored antioxidant levels and reduced MDA effectively. SM showed a dose-dependent effect, with SM-H better than SM-L. Notably, SMD, particularly at the high dose (SMD-H, 200 mg per kg b.w.), exhibited a comparable restoration of antioxidant markers to that of silymarin, showing a significant increase in CAT, GSH, GPx, and SOD, and a notable reduction in MDA levels. These outcomes highlight the protective role of the treatments in reducing oxidative stress and liver injury triggered by paracetamol toxicity (Fig. 8).

2.4.3 Effect on NRF2, γ-GCS, HO-1, and pro-inflammatory cytokines (TNF-α, IL-6). ELISA analysis showed that the PCM group had a significant ($P < 0.0001$) decrease in the levels of NRF2, γ-GCS, and HO-1 compared to the normal group, indicating impaired activation of the antioxidant response and reduced detoxification capacity. Conversely, pro-inflammatory markers TNF-α ($P < 0.0001$) and IL-6 ($P < 0.0001$) were significantly elevated in the PCM group, consistent with oxidative stress and inflammation. Treatment with SMD restored antioxidant defense, as shown by the upregulation of NRF2, γ-GCS,

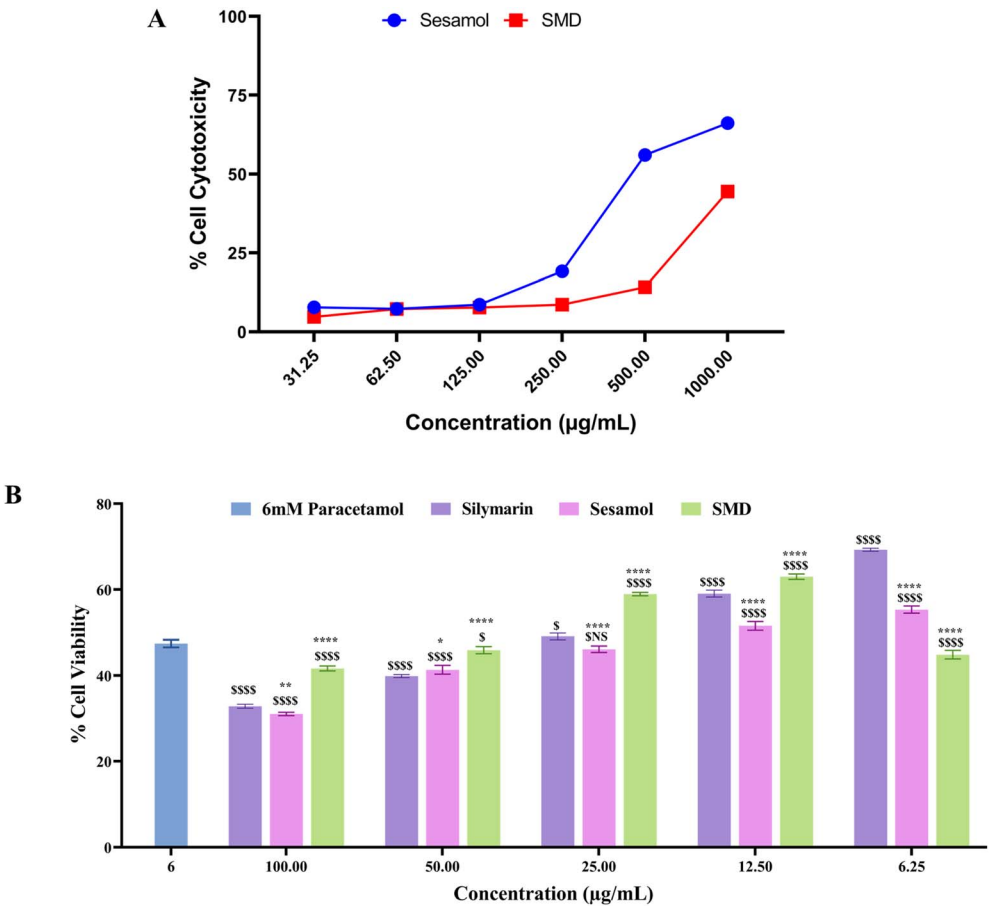

Fig. 6 (A) % cell cytotoxicity *vs.* concentration graph of the compounds and (B) % cell viability *vs.* concentration graph of standard and test compounds. The values are expressed as mean ± SD ($n = 3$). Statistical analysis was conducted using one-way ANOVA followed by Tukey's post hoc test. Significance indicators were as follows: $^{\$}P \leq 0.05$, $^{\$\$\$\$}P \leq 0.0001$, $^{\$}$NS = non-significant *vs.* paracetamol group, $^{*}P \leq 0.05$, $^{**}P \leq 0.01$, $^{****}P \leq 0.0001$ *vs.* silymarin group.

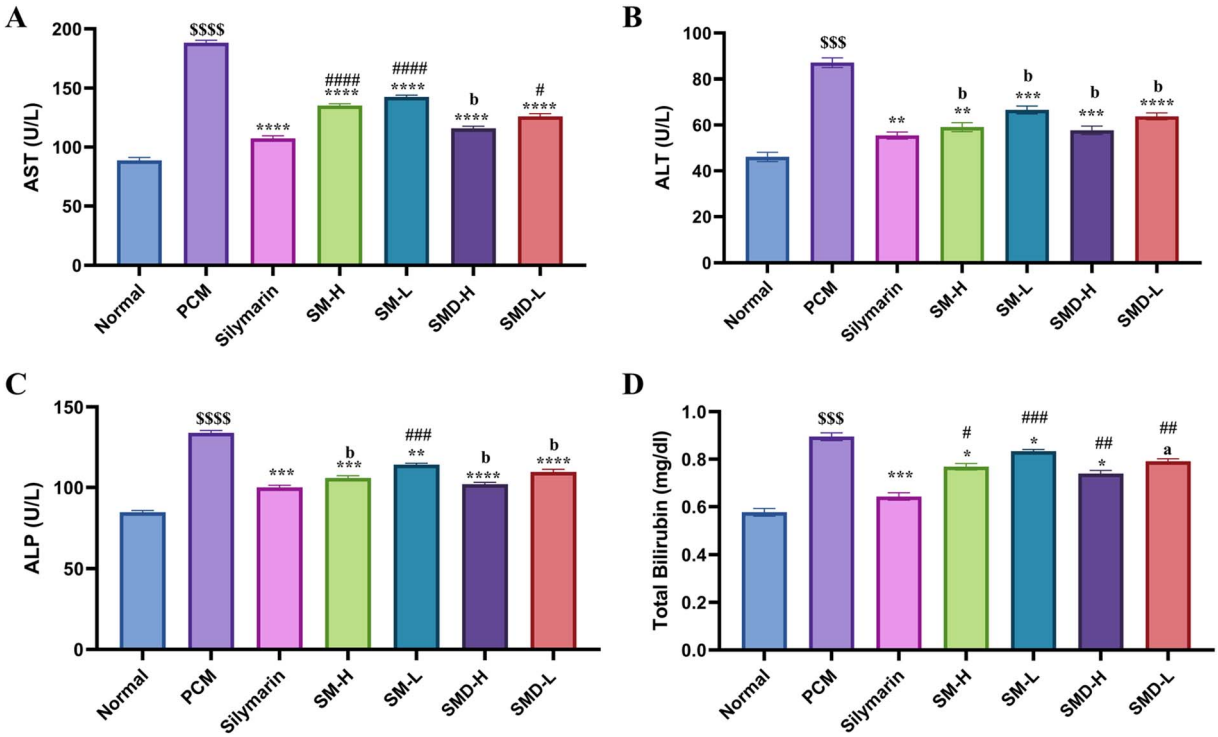

Fig. 7 Serum biochemical parameters in terms of (A) AST, (B) ALT, (C) ALP, and (D) total bilirubin after 7 days of treatment and PCM exposure. Data is present in mean ± SEM, $^{\$\$\$\$}P \leq 0.0001$, $^{\$\$\$}P \leq 0.001$, $^{\$\$}P \leq 0.01$, $^{\$}P \leq 0.05$ *vs.* normal control, $^{****}P \leq 0.0001$, $^{***}P \leq 0.001$, $^{**}P \leq 0.01$, $^{*}P \leq 0.05$ *vs.* PCM group, $^{\#\#\#\#}P \leq 0.0001$, $^{\#\#\#}P \leq 0.001$, $^{\#\#}P \leq 0.01$, $^{\#}P \leq 0.05$ *vs.* silymarin. ^{a}P non-significant *vs.* PCM group, ^{b}P non-significant *vs.* silymarin group.

and HO-1, while simultaneously suppressing TNF-α and IL-6. Notably, SMD at high dose produced a greater increase in antioxidant markers than both sesamol (SM) and silymarin, and also demonstrated stronger suppression of inflammatory cytokines than SM alone, with efficacy comparable to silymarin (Fig. 9).

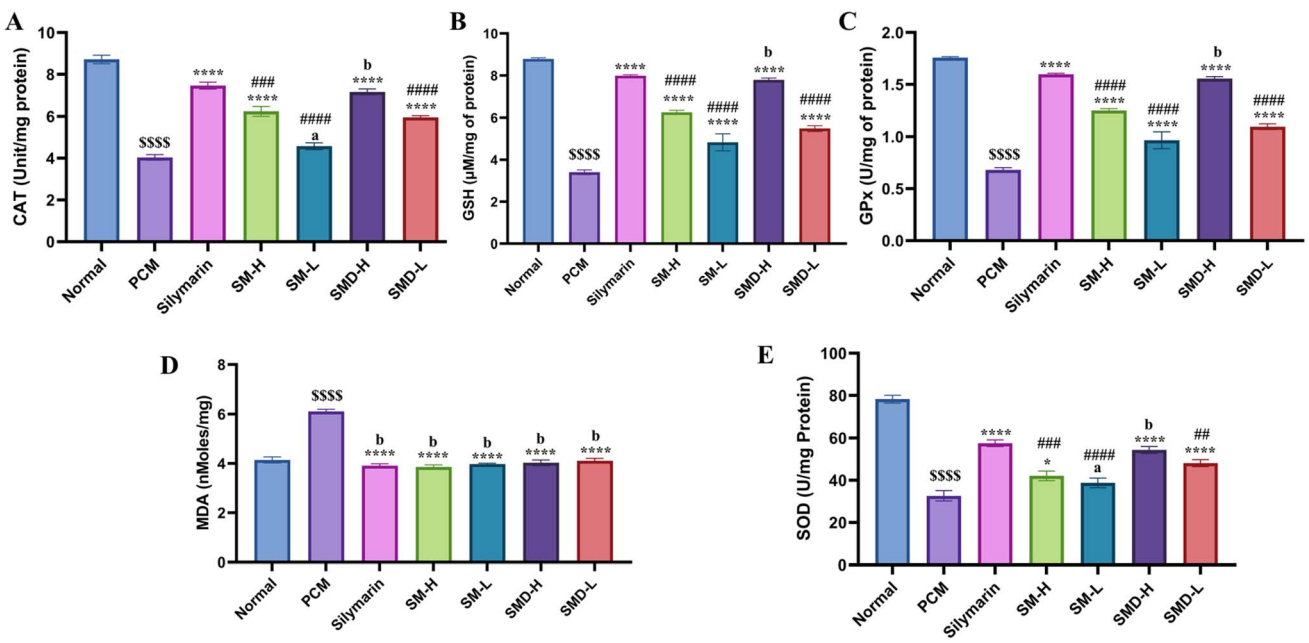

Fig. 8 Antioxidant parameters in terms of (A) CAT, (B) GSH, (C) GPx, (D) MDA, and (E) SOD after 7 days of treatment and PCM exposure. Data is present in mean ± SEM, $^{\$\$\$\$}P \leq 0.0001$, $^{\$\$\$}P \leq 0.001$, $^{\$\$}P \leq 0.01$, $^{\$}P \leq 0.05$ *vs.* normal control, $^{****}P \leq 0.0001$, $^{***}P \leq 0.001$, $^{**}P \leq 0.01$, $^{*}P \leq 0.05$ *vs.* PCM group, $^{\#\#\#\#}P \leq 0.0001$, $^{\#\#\#}P \leq 0.001$, $^{\#\#}P \leq 0.01$, $^{\#}P \leq 0.05$ *vs.* silymarin. ^{a}P non-significant *vs.* PCM group, ^{b}P non-significant *vs.* silymarin group.

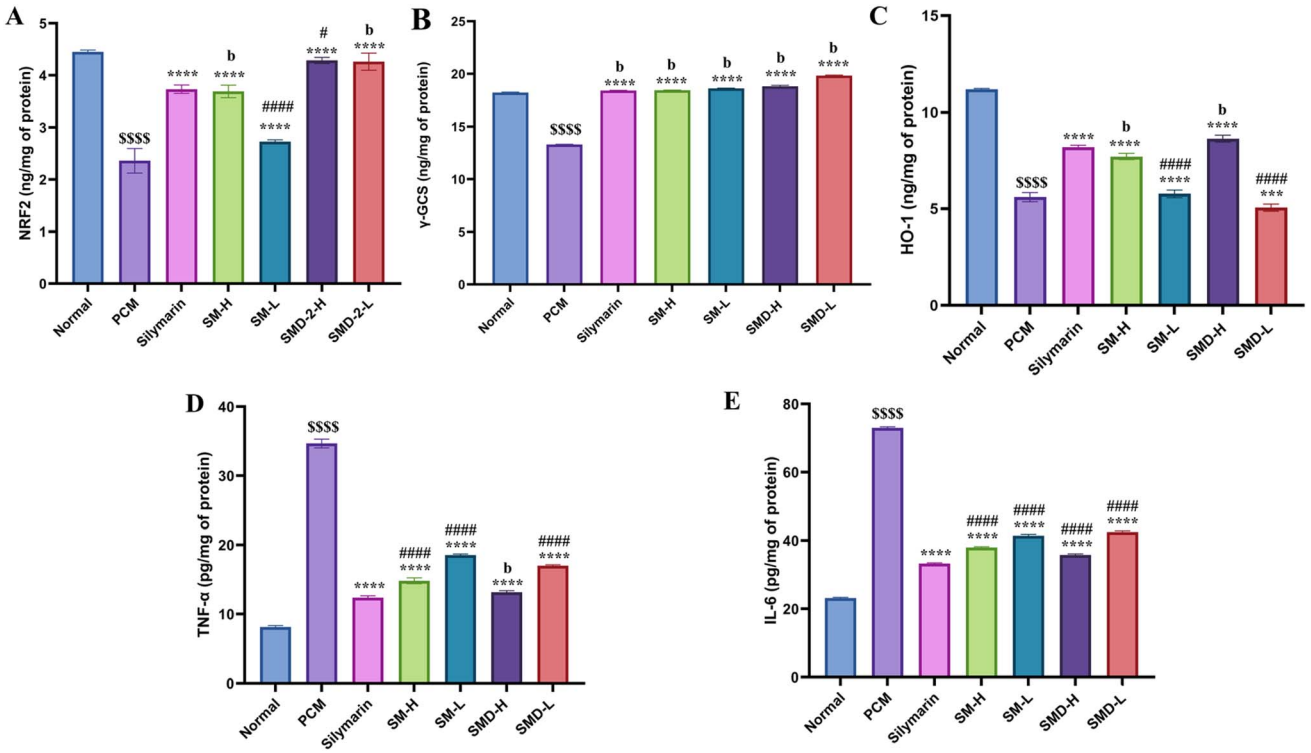

Fig. 9 Mechanistic pathway and inflammatory markers in terms of (A) NRF-2, (B) γ-GCS, (C) HO-1, (D) TNF-α, and (E) IL-6 after 7 days of treatment and PCM exposure. Data is present in mean ± SEM, $^{\$\$\$\$}P \leq 0.0001$, $^{\$\$\$}P \leq 0.001$, $^{\$\$}P \leq 0.01$, $^{\$}P \leq 0.05$ *vs.* normal control, $^{****}P \leq 0.0001$, $^{***}P \leq 0.001$, $^{**}P \leq 0.01$, $^{*}P \leq 0.05$ *vs.* PCM group, $^{\#\#\#\#}P \leq 0.0001$, $^{\#\#\#}P \leq 0.001$, $^{\#\#}P \leq 0.01$, $^{\#}P \leq 0.05$ *vs.* silymarin. ^{a}P non-significant *vs.* PCM group, ^{b}P non-significant *vs.* silymarin group.

Although western blotting or PCR are widely used to assess gene and protein expression, ELISA provides a reliable quantitative measure of protein levels and has been extensively validated in pharmacological studies. In this work, the use of commercial ELISA kits enabled accurate assessment of NRF2, HO-1, and inflammatory cytokines, and the results were consistent with biochemical and histopathological findings. Based on these findings, we cautiously describe SMD as a potential NRF2 activator, supported by computational modeling and indirect biological evidence (ELISA upregulation of NRF2, HO-1, and γ-GCS). While direct biochemical confirmation of KEAP1–NRF2 disruption (*e.g.*, western blotting or pull-down assays) was not performed, the clear dose-dependent upregulation of NRF2 and HO-1 strongly suggests pathway activation. Future studies will aim to provide direct mechanistic evidence for KEAP1–NRF2 modulation by SMD.

2.4.4 Histological assessment of hepatic injury using H&E staining and grading system. A semi-quantitative scoring system (0–5 scale) was employed to assess the severity of liver damage observed in H&E-stained sections. Each parameter; necrosis, inflammatory infiltrate, vacuolar degeneration, and sinusoidal dilation, was graded based on extent and intensity, with 0 indicating absence and 5 indicating severe pathology. Scores were inferred from qualitative histological observations and used to evaluate the hepatoprotective efficacy of treatments comparatively. Lower scores reflect better preservation of hepatic architecture (Table 2).

Liver damage due to oxidative and inflammatory insults was assessed through histopathological examination using

Table 2 Histopathological scores of liver tissue following paracetamol-induced hepatotoxicity and treatment with silymarin, sesamol, and SMD[a]

Group	Necrosis	Inflammatory infiltrate	Vacuolar degeneration	Sinusoidal dilation
Normal control	0	0	0	0
PCM group	2	5	5	5
Standard group (silymarin)	1	3	2	2
Sesamol high dose	2	2	2	3
Sesamol low dose	0	2	1	2
SMD high dose	0	1	0	1
SMD low dose	0	1	0	1

[a] 0 = absent (normal), 1–2 = mild, 3 = moderate, 4–5 = severe. $n = 3$.

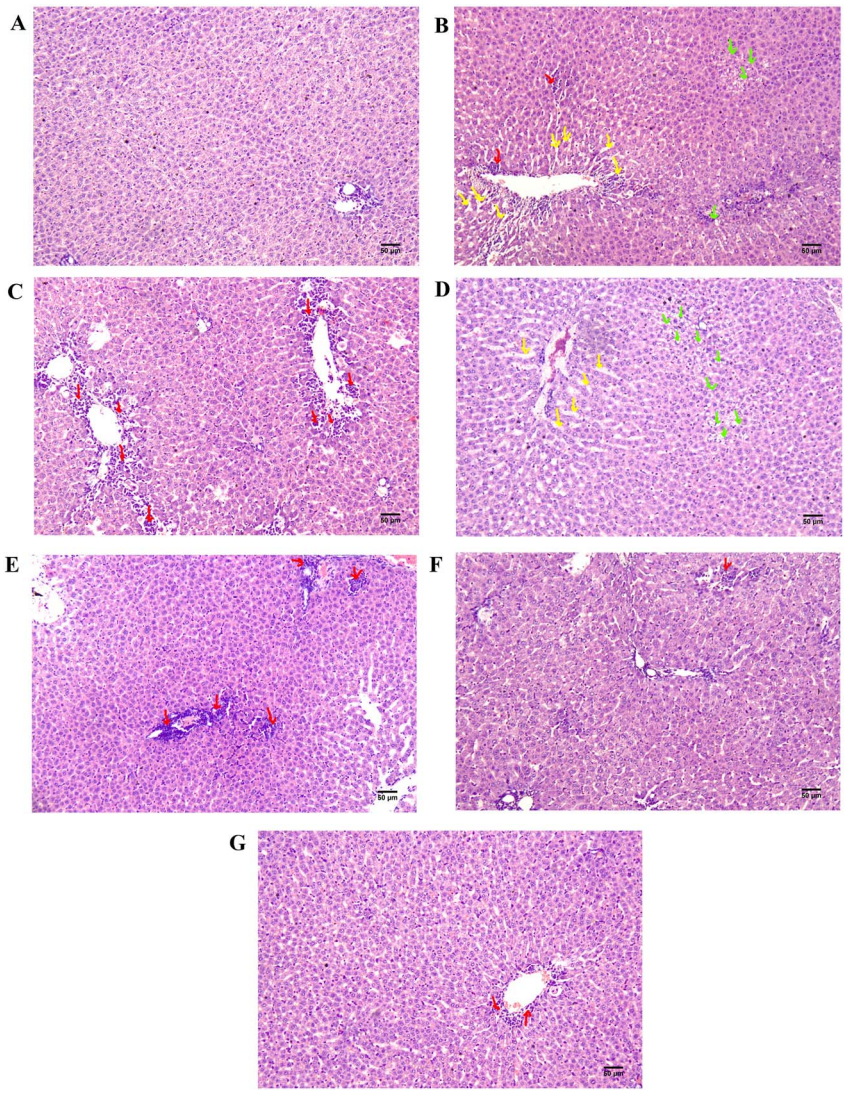

Fig. 10 Effect on hepatic histology rat liver by PCM-induced toxicity (Hematoxylin–Eosin (H&E) staining). (A) Normal group, (B) PCM group, (C) standard group (silymarin), (D) sesamol high dose group (SM-H), (E) sesamol low dose group (SM-L), (F) SMD-H (high dose), and (G) SMD-L (low dose). The Red, yellow, and green arrow signifies inflammatory infiltrates, dilation of Sinusoids, and vacuolar degeneration, respectively.

hematoxylin and eosin (H&E) staining. In the normal control group (Fig. 10A), hepatic tissue exhibited well-preserved architecture with intact hepatocyte morphology and no signs of inflammation, vacuolar degeneration, or sinusoidal dilation. However, in the paracetamol group (Fig. 10B), extensive hepatic injury was observed. These included marked inflammatory cell infiltration (red arrows), sinusoidal dilation (yellow arrows), and pronounced vacuolar degeneration (green) alongside apoptotic hepatocytes and early necrotic changes, reflecting severe hepatocellular damage.

Among the treatment groups, the silymarin-treated group (Fig. 10C) showed modest restoration of hepatic integrity, with a noticeable reduction in inflammatory infiltrates and sinusoidal dilation. However, mild vacuolar changes and apoptotic bodies remained. The SM high-dose group (Fig. 10D) demonstrated partial hepatoprotection, characterized by reduced inflammation and sinusoidal dilation, although necrosis and cellular degeneration were still evident. The SM low-dose group (Fig. 10E) offered better consistency, showing the absence of necrosis and vacuolation, with reduced inflammation and sinusoidal dilation, indicating moderate tissue preservation. In the SMD high-dose group (Fig. 10F), liver sections lacked necrosis entirely, with only mild inflammatory infiltration and sinusoidal dilation observed. Vacuolation was absent in the remaining tissue, suggesting a superior protective effect relative to both SM doses. The SMD low-dose group (Fig. 10G) displayed further improved histoarchitecture, with the absence of necrosis and vacuolar changes across all sections and a marked reduction in inflammatory infiltrates and sinusoidal dilation. These indicated that even at a lower dose, SMD was able to preserve hepatic structure more effectively than SM and comparably to silymarin.

Collectively, these findings highlight the enhanced hepatoprotective efficacy of the SMD, particularly at the higher

Table 3 Experimental design, treatment schedule, and sampling timeline in the PCM-induced hepatotoxicity model

Group	Treatment	Dose (mg per kg b.w., p.o.)	Treatment period (days 1–7)	PCM administration (day 7)	Sampling (after PCM)
I	Normal control	0.25% CMC	Vehicle daily for 7 days	—	48 h post-last dose
II	PCM control	2500 mg per kg b.w., p.o.	Vehicle daily for 7 days	Single PCM dose on day 7	48 h post-PCM
III	Silymarin	100 mg per kg b.w., p.o.	Silymarin daily for 7 days	PCM (2.5 g kg^{-1}) 1 h after last dose	48 h post-PCM
IV	Sesamol low-dose (SM-L)	100 mg per kg b.w., p.o.	Sesamol daily for 7 days	PCM (2.5 g kg^{-1}) 1 h after last dose	48 h post-PCM
V	Sesamol high-dose (SM-H)	200 mg per kg b.w., p.o.	Sesamol daily for 7 days	PCM (2.5 g kg^{-1}) 1 h after last dose	48 h post-PCM
VI	SMD low-dose (SMD-L)	100 mg per kg b.w., p.o.	SMD daily for 7 days	PCM (2.5 g kg^{-1}) 1 h after last dose	48 h post-PCM
VII	SMD high-dose (SMD-H)	200 mg per kg b.w., p.o.	SMD daily for 7 days	PCM (2.5 g kg^{-1}) 1 h after last dose	48 h post-PCM

dose, which not only prevented paracetamol-induced histological damage but also performed either on par with or better than the reference standard, silymarin. This supports the hypothesis that structural modification of SM into SMD yields a compound with improved therapeutic potential against liver injury (Fig. 10).

3. Conclusion

The present study presents a comprehensive evaluation of the hepatoprotective potential of the sesamol derivative (SMD) against PCM-induced liver injury. The compound was synthesized through a targeted modification of the sesamol structure and thoroughly characterized *via* FTIR, LC-MS, ^{1}H NMR, and ^{13}C NMR, confirming its structural integrity. The biological evaluation revealed that SMD exhibited potent antioxidant activity with an IC_{50} value of 32.79 μg mL^{-1}, representing a 4.5-fold enhancement over the parent sesamol (IC_{50}: 148.86 μg mL^{-1}). Furthermore, *in vitro* assessment in HepG2 cells against paracetamol induced toxicity, demonstrated that SMD achieved maximum protection of 62.99% and 58.92% at 12.25 μg mL^{-1} and 25 μg mL^{-1}, respectively, significantly outperforming sesamol, which offered 55.31% protection at 12.5 μg mL^{-1}.

In vivo studies further validated the protective effects of SMD, particularly at a dose of 200 mg kg^{-1}, which effectively mitigated serum levels of hepatic biomarkers, including AST, ALT, ALP, and total bilirubin, comparable to the hepatoprotective reference drug, silymarin. Additionally, SMD markedly restored antioxidant enzyme levels (CAT, GSH, GPx, SOD) while attenuating MDA levels, underscoring its antioxidant efficacy *in vivo*. Histopathological analysis corroborated these findings, demonstrating substantial improvement in hepatic architecture, characterized by reduced necrosis, sinusoidal dilation, and inflammatory infiltration in SMD-treated groups.

Mechanistic studies revealed that SMD significantly activated the NRF2/HO-1 pathway, as evidenced by the upregulation of NRF2, HO-1, and γ-GCS in liver tissues. This activation was associated with a concomitant reduction in TNF-α and IL-6, suggesting that the hepatoprotective effects of SMD are mediated, at least in part, through NRF2-dependent antioxidant and anti-inflammatory pathways. Complementary molecular-docking and molecular-dynamics analyses further indicated that SMD interacts within the KEAP1–NRF2 binding region (PDB 4L7D, ligand 1VX), providing computational support for the observed NRF2 activation. Collectively, these findings position SMD as a promising hepatoprotective agent with potential utility in mitigating DILI through NRF2 pathway modulation, warranting further pharmacological and mechanistic studies. Further pharmacokinetic profiling and dose optimization will be necessary before translational application.

4. Experimental

4.1 General information

All the chemicals, reagents, and solvents used in this study were of molecular, analytical, and synthetic grades commercially available in Sigma, SRL, Thermo Fisher Scientific. TLC silica gel 60 F_{254} was supplied by Supelco. In addition to these chemicals and reagents, various diagnostic kits were employed in the study. The SGOT Nanoplus Kit, SGPT Nanoplus Kit, ALP Nanoplus Kit, total protein kit, albumin Nanoplus Kit, bilirubin direct kit, and total bilirubin kit were all obtained from Agappe. Elisa kits such as Rat TNF-α, Rat IL-6, Rat NRF2, Rat γ-glutamylcysteine synthetase, Rat HO-1 was obtained from Krishgen Biosystems.

4.2 Molecular docking and molecular dynamics simulation studies

Computational calculations were performed through the GUI of Schrödinger 2024-2, utilizing Maestro version-14 and analysis using various modules such as for Pathfinder module "Reaction-based enumeration" for generating focused virtual library of compounds, for molecular docking the Glide module "Ligand docking", Prime module "MM-GBSA" for MM-GBSA calculation, "QikProp" for ADME studies and "Desmond" for MDS studies.

4.2.1 Reaction-based enumeration, protein preparation, and docking analysis. The Schrödinger suite's Pathfinder module was employed for compound design using the

"Reaction-Based Enumeration" tool. The process involved selecting the "Reaction Library" and choosing the amide coupling reaction, where 2-(benzo[*d*][1,3]dioxol-5-yloxy)acetic acid was defined as one reactant. The second reactant was selected from a custom library of 21 primary and secondary amines available in the laboratory. The enumeration option was then applied to generate the compound library. The KEAP1–NRF2 protein structure, PDB-4L7D was retrieved from the PDB and it has 1VX as co-crystallized ligand with a resolution of 2.25 Å. Protein preparation was performed using Schrödinger's "Protein Preparation Workflow," involving preprocessing, H-bond optimization, energy minimization using the OPLS4 force field, and removed water molecules extending 5 Å. Receptor grid generation was done at $X = -22.79$, $Y = 39.11$, and $Z = -36.57$, with functional residues maintained.

The virtual library generated through reaction-based enumeration was processed using the LigPrep tool under OPLS4 force field at pH 7.4. Only one stereoisomer was generated per ligand. Docking was performed at physiological pH (7.4) using implicit solvent conditions. To ensure reliability, docking was conducted in triplicate, and the best-ranked pose (lowest GlideScore and RMSD < 1.0 Å) was selected for further analysis. Molecular docking was conducted utilizing GLIDE in three stages: HTVS, SP, and XP. Post-docking minimization and RMSD calculations were applied to assess binding affinity.[23–26]

Binding-free energy was estimated using MM-GBSA *via* the Prime module, applying the formula:

$$\Delta G(\text{binding}) = \Delta E(\text{MM}) + \Delta G(\text{SA}) + \Delta G(\text{solvation}),$$

where ΔG(SA), ΔE(MM), and ΔG(solvation) represent surface area energy, minimized energy, and solvation energy differences between the complex and its unbound components, respectively.[27]

4.2.2 Absorption, distribution, metabolism & excretion (ADME) and drug-likeness. "QikProp" module was used for predicting ADME parameters and assess drug-likeness in accordance with Lipinski's rule of five.

4.2.3 Molecular dynamic simulations (MDS). MDS studies were employed to examine the functioning and the dynamics of ligand–protein complexes. Molecular docking studies don't mimic the body's biological environment as the protein and ligands were suspended in water, therefore, it was used for addressing this concern. Utilizing Desmond's "System Builder" module, wherein the protein–ligand complex was situated within a "simple point charge" solvent framework, neutralized with Na^+/Cl^- counterions. The ionic strength was maintained at 0.15 M to simulate physiological conditions. All simulations were carried out at physiological pH (7.4). The boundary conditions were established as orthorhombic, and the buffer method was used to determine the box size, with a set size of 10 Å for each of *a*, *b*, and *c*, while angles α, β, and γ were maintained at 90°. The OPLS4 force field was applied, followed by system minimization using the minimization tool. For the MDS setup, the "Molecular Dynamics" module of Desmond was utilized with a simulation duration of 500 ns, recording trajectory frames every 100 picoseconds, resulting in 1000 frames. The *NPT* ensemble was selected, maintaining a constant particle number, a pressure of 1.01325 bar, and a temperature of 300 K.[28] Simulation stability was visually inspected, and reproducibility of RMSD and RMSF profiles was confirmed through repeat trajectory minimization. Upon completion, the "Simulation Interaction Diagram" module was used for report generation. Post-MDS analysis involved evaluating parameters such as RMSD, RMSF, FEL, PCA, TE, rGyr, SASA, and MM-GBSA ΔG bind.

4.3 Synthesis and characterization of 3-(2-(benzo[*d*][1,3] dioxol-5-yloxy)acetamido)benzoic acid (SMD)

4.3.1 Synthesis of SMD. Ethyl 3-(2-(benzo[*d*][1,3]dioxol-5-yloxy)acetamido)benzoate (7 g) was dissolved in ethanol (70 mL), and 1 M NaOH solution (35 mL) was added. The reaction was carried out under a normal laboratory atmosphere with continuous magnetic stirring. Reaction progress was monitored by thin-layer chromatography (TLC) using ethyl acetate : *n*-hexane (2 : 8 v/v) as the mobile phase, and completion was confirmed by disappearance of the starting ester spot. The reaction mixture was refluxed for 2 hours under continuous stirring to hydrolyze the ester group. After completion, the mixture was concentrated under reduced pressure and poured into ice-cold water. The resulting solid was filtered, washed thoroughly with distilled water to remove residual alkali, and dried at 55 °C to obtain 3-(2-(benzo[*d*][1,3]dioxol-5-yloxy) acetamido)benzoic acid.[29] The yield was 90% with off white solid and MP was 190–192 °C.

4.3.2 Characterization of SMD. FTIR (KBr, cm^{-1}): 3338.78 (O–H stretch, carboxylic acid), 3273.20 (N–H stretch, secondary amide), 1691.57 and 1672.2 (C=O stretch, carboxylic acid and amide groups); ^{1}H NMR (400 MHz, DMSO) δ 13.01 (s, 1H), 10.22 (s, 1H), 8.30 (t, $J = 1.9$ Hz, 1H), 7.89 (dd, $J = 8.1$, 2.1 Hz, 1H), 7.67 (dt, $J = 7.7$, 1.4 Hz, 1H), 7.46 (t, $J = 7.9$ Hz, 1H), 6.84 (d, $J = 8.5$ Hz, 1H), 6.74 (d, $J = 2.6$ Hz, 1H), 6.45 (dd, $J = 8.5$, 2.6 Hz, 1H), 5.98 (s, 2H), 4.64 (s, 2H); ^{13}C NMR (101 MHz, DMSO) δ 167.57, 167.40, 153.60, 148.36, 142.15, 139.05, 131.76, 129.47, 124.99, 124.36, 121.00, 108.46, 106.48, 101.61, 98.68, 68.48; ITMS: For $C_{16}H_{13}NO_6$, mass 315.07 detected as *m*/*z* 316.06.15 ($[M + H]^+$) and *m*/*z* 314.06 ($[M - H]^-$).

Analytical TLC displayed a single spot ($R_f = 0.25$ in ethyl acetate : *n*-hexane = 2 : 8 v/v), and no additional peaks were observed in the NMR and LC-MS spectra, confirming the purity of SMD obtained as a single major component suitable for biological evaluation.

Synthesis and characterization of ethyl 3-(2-(benzo[*d*][1,3] dioxol-5-yloxy)acetamido)benzoate is given in SI.

4.4 *In vitro* antioxidant, cytotoxicity, and protective activity against paracetamol (PCM)-Induced toxicity assay

4.4.1 Antioxidant activity of compounds using DPPH assay. The antioxidant potential of compounds was evaluated using the DPPH (1,1-diphenyl-2-picrylhydrazyl) assay in the concentration range of 15.625, 31.25, 62.5, 125, 250, 500, and 1000 μg mL^{-1} following the method described by F. Abu.[30]

4.4.2 Cell cytotoxicity assay of test compounds on HepG2 cell line by SRB assay. HepG2 cells were obtained from the National Centre for Cell Science (NCCS), Pune, India. The cells were cultured in Dulbecco's Modified Eagle Medium (DMEM) supplemented with 10% fetal bovine serum (FBS) and 1% antibiotic–antimycotic solution. The cultures were maintained in T25 flasks at 37 °C in a humidified incubator with 5% CO_2 atmosphere, and the media were renewed every 48 hours.

As SMD was poorly soluble in PBS (pH 7.4), the test compound was solubilized in 20 μL of dimethyl sulfoxide (DMSO) and subsequently diluted with the appropriate culture medium to yield a stock solution of 1 mg mL^{-1}. The desired working concentrations were prepared by further serial dilution with the medium, ensuring that the final DMSO concentration did not exceed 0.5% (v/v). The compounds were diluted in maintenance medium to achieve final concentrations of 15.625, 31.25, 62.5, 125, 250, 500, and 1000 μg mL^{-1}. For the assay setup, 100 μL of medium containing 8×10^3 cells was dispensed into each well of a 96-well plate, followed by a 24 hour incubation period. Subsequently, 100 μL of the prepared compound solutions were added to the wells, and the plates were incubated for an additional 48 hours. SRB assay was performed based on the method described by E. Orellana.[31]

Percent cell cytotoxicity is calculated using the formula:

$$\%\ \text{cell cytotoxicity} = \left[\frac{(\text{absorbance of control} - \text{absorbance of test})}{\text{absorbance of control}}\right] \times 100$$

4.4.3 Cell protective assay. After seeding, HepG2 cells were allowed to adhere and stabilize under standard conditions (37 °C, 5% CO_2, humidified atmosphere) for 24 hours. The cells were then pretreated with test compounds for 24 hours. Following pretreatment, the culture medium was replaced with fresh medium containing 6.5 mM paracetamol (PCM) to induce toxicity, and the plates were incubated for an additional 48 hours under the same culture conditions.

$$\%\ \text{cell viability} = 100 - \left[\frac{(\text{absorbance of blank} - \text{absorbance of test})}{\text{absorbance of blank}} \times 100\right]$$

% cell viability was calculated using the formula:

4.5 *In vivo* evaluation of hepatoprotective potential

4.5.1 Experimental design and PCM-induced liver injury model. Female albino Wistar rats (180–220 gram b.w.) of 8–12 weeks were maintained at Central Animal Research Facility, Manipal Academy of Higher Education (MAHE), Manipal, Karnataka, India, at temperature 23 + 2 °C, under controlled relative humidity (50 ± 5%), and 12:12 hour light and dark cycle were used in the study. All animal procedures were performed in accordance with CPCSEA guidelines and approved by the Institutional Animal Ethics Committee of Kasturba Medical College, MAHE, Manipal, Karnataka, India with IAEC no. IAEC/KMC/08/2022.

Acute oral toxicity of SMD was assessed in accordance with OECD guideline 425,[32] and based on the findings, two doses; 100 mg kg^{-1} (low) and 200 mg kg^{-1} (high), were selected for *in vivo* studies. Hepatotoxicity was induced in female albino Wistar rats using paracetamol (PCM; 2.5 g kg^{-1}, p.o.) on day 7.[33] Animals were randomly divided into seven groups ($n = 6$) as described in Table 3.

After 48 hours of PCM administration, animals were anaesthetized with diethyl ether, and blood was collected *via* retro-orbital puncture for biochemical and cytokine estimation. The rats were then euthanized, and livers were excised, rinsed with cold PBS, blotted dry, weighed, and processed for antioxidant enzyme analysis and histopathological examination.

4.5.2 Biochemical analysis. Biochemical parameters including AST, ALT, total and direct bilirubin, ALP, total protein, and albumin were measured from the liver homogenate supernatant using a fully automated analyzer (Agappe Mispa Ace). Calibration was performed automatically by the analyzer using the manufacturer-supplied calibration reagents and reference standards to ensure accuracy and linearity of measurements before each run. Serum levels of tumor necrosis factor-α (TNF-α) and interleukin-6 (IL-6) were quantified using ELISA kits from Krishgen Biosystems.

4.5.3 Antioxidant studies

4.5.3.1 Assay for catalase.[34] The activity of catalase (CAT) was assessed in accordance with the protocol established by Beers *et al.*,[34] 1984. A volume of 50 μL of tissue homogenate was introduced into a solution comprising phosphate buffer (pH 7.0) and H_2O_2 (with a final optical density ranging from 3 to 5). The variation in absorbance was measured over a period of one minute at a wavelength of 240 nm. The catalase activity was subsequently quantified and expressed in units per milligram protein.

4.5.3.2 Assay for super oxide dismutase (SOD).[35] A mixture containing 50 μL of tissue homogenate, carbonate buffer (1850 μL), and adrenaline (100 μL) was prepared directly inside cuvette. The change in absorbance at 480 nm over 60 seconds ($A_0 - A_{60}$) was recorded. The activity of SOD was evaluated by comparing absorbance fluctuations in relation to a standard curve and quantified in units per milligram of protein (U per mg protein).

4.5.3.3 Assay for glutathione.[36] It was conducted by assessing the chromatic development resulting from the formation of derivatives *via* DTNB. Tissue homogenate and 5% TCA was taken in equal volume and subsequently centrifuged to obtain a transparent supernatant. The resultant solution (500 μL of supernatant, 500 μL of DTNB and 3 mL of PBS) was incubated for a duration of 10 minutes at an ambient temperature. The

absorbance was measured at 412 nm. The concentration of glutathione was determined by extrapolating from a standard curve and reported in μmole per mg of protein.

4.5.3.4 Assay of glutathione peroxidase (GPx) activity.[37] The assay reaction mixture (1 mL) should contain 50 mM phosphate buffer (pH 7.0), 2.1 mM reduced glutathione, 1 U per mL glutathione reductase, 0.25 mM NADPH, 0.25 mM H_2O_2, and 0.1 mL of the tissue homogenate. The reaction is initiated by adding H_2O_2, and the decrease in absorbance at 340 nm is monitored for 3–5 minutes using a UV-visible spectrophotometer. GPx activity is calculated using the molar extinction coefficient of NADPH ($\varepsilon = 6.22 \times 10^3\ M^{-1}\ cm^{-1}$) and expressed as units per milligram of protein (U per mg protein), where one unit of GPx activity corresponds to the oxidation of 1 μmol of NADPH per minute.

4.5.3.5 Assay of lipid peroxidation.[38] An equal volume of tissue homogenate (0.5 mL) and a reagent mixture containing TBA, TCA, and BHT was mixed, then incubated for 10 minutes at 90 °C. After heating, the mixture were centrifuged for 5 minutes at 5000 rpm, and the supernatant absorbance was recorded at 530 nm. Lipid peroxidation was quantified based on malondialdehyde levels and expressed as nanomoles per milligram.

4.5.3.6 Effect on NRF2, γ-GCS, HO-1, and pro-inflammatory cytokines (TNF-α, IL-6). Elisa kits were purchased from Krishgen Biosystems and estimated using the company instructions.

4.6 Histological study

Livers were preserved in a 10% formalin solution for 24 to 48 hours, followed by macroscopic assessment. Subsequently, liver tissue was dehydrated through graded ethanol (70%, 90%, and 100%) and cleared in xylene. The samples were infiltrated with molten paraffin wax and embedded to prepare tissue blocks. Sections of approximately 4 μm thickness were cut using a rotary microtome, floated on a warm water bath (50–52 °C), and mounted on glass slides. The sections were deparaffinized in xylene (two changes, 5 min each), rehydrated through descending grades of ethanol (100%, 90%, and 70%), and stained with hematoxylin for 2 min and eosin for 1 min. After washing in running water and dehydration with absolute alcohol, slides were cleared in xylene and mounted using DPX. Histological evaluation was performed using an LX-500 LED trinocular research microscope (Labomed) at 100× magnification. Images were captured using a MiaCam CMOS AR 6Pro microscope camera integrated with Image A.R. Pro software (scale bar = 50 μm).

4.7 Statistical analysis

The data were evaluated employing one-way ANOVA within the GraphPad Prism software, subsequently accompanied by Tukey's post hoc analysis. Prior to ANOVA, data were checked for normal distribution and homogeneity of variance using the built-in tests in GraphPad Prism to ensure suitability for parametric analysis. All *in vitro* experiments were performed in triplicate ($n = 3$) and expressed as mean ± SD, while *in vivo* experiments were conducted with six animals per group ($n = 6$) and expressed as mean ± SEM. A p-value of less than 0.05 was considered statistically significant. Levels of statistical significance were indicated as follows: $p < 0.05$, $p < 0.01$, $p < 0.001$, and $p < 0.0001$. The symbols used in figures denote comparisons as follows: $ (*vs.* normal control), * (*vs.* PCM group), and # (*vs.* silymarin group), while "a" and "b" represent non-significant differences.

Author contributions

Ajay Mili: conceptualization, methodology, investigation, data curation, writing – original draft preparation, writing – reviewing and editing. Sumit Birangal: methodology, investigation, data curation. Krishnadas Nandakumar: supervision, data curation, writing – reviewing and editing. Raghu Chandrashekar Hariharapura: investigation, data curation. Nitesh Kumar: investigation, data curation. Aravinda Pai: investigation, data curation. Richard Lobo: supervision, data curation, writing – reviewing and editing. All authors reviewed the manuscript.

Conflicts of interest

The authors declare that they have no known competing financial interests or personal relationships that could have appeared to influence the work reported in this paper.

Data availability

Data will be made available on request.

Supplementary information (SI) is available. See DOI: https://doi.org/10.1039/d5ra07867a.

Acknowledgements

Author Ajay Mili and Sumit Birangal are thankful to the Manipal Academy of Higher Education (MAHE) for providing Dr T. M. A. Pai Doctoral Fellowship. The authors also acknowledge with thanks the Manipal College of Pharmaceutical Sciences (MCOPS), the Manipal-Schrödinger Centre for Molecular Simulations and the Manipal Academy of Higher Education (MAHE) for providing facilities for this work.

References

1 R. J. Andrade, N. Chalasani, E. S. Björnsson, A. Suzuki, G. A. Kullak-Ublick, P. B. Watkins, H. Devarbhavi, M. Merz, M. I. Lucena, N. Kaplowitz and G. P. Aithal, *Nat. Rev. Dis. Primers*, 2019, **5**, 58.
2 A. Mili, S. Birangal, K. Nandakumar and R. Lobo, *Mol. Diversity*, 2024, **28**, 1709–1731.
3 A. Regev, M. Palmer, M. I. Avigan, L. Dimick-Santos, W. R. Treem, J. F. Marcinak, D. Seekins, G. Krishna, F. A. Anania, J. W. Freston, J. H. Lewis, A. J. Sanyal and N. Chalasani, *Aliment. Pharmacol. Ther.*, 2019, **49**, 702–713.
4 L. Yuan and N. Kaplowitz, *Clin. Liver Dis.*, 2013, **17**, 507–518.

5 M. Villanueva-Paz, L. Morán, N. López-Alcántara, C. Freixo, R. J. Andrade, M. I. Lucena and F. J. Cubero, *Antioxidants*, 2021, **10**, 390.
6 J. Das, J. Ghosh, A. Roy and P. C. Sil, *Toxicol. Appl. Pharmacol.*, 2012, **260**, 35–47.
7 A. Raghunath, R. Nagarajan, K. Sundarraj, K. Palanisamy and E. Perumal, *Basic Clin. Pharmacol. Toxicol.*, 2019, **125**, 259–270.
8 Y. Wang, X. Fu, L. Zeng, Y. Hu, R. Gao, S. Xian, S. Liao, J. Huang, Y. Yang, J. Liu, H. Jin, J. Klaunig, Y. Lu and S. Zhou, *Commun. Biol.*, 2024, **7**, 621.
9 J. Zhou, Q. Zheng and Z. Chen, *Front. Cell Dev. Biol.*, 2022, **10**, 826204.
10 C. Mayer, L. Riera-Ponsati, S. Kauppinen, H. Klitgaard, J. T. Erler and S. N. Hansen, *Front. Pharmacol*, 2024, **15**, 1437939.
11 A. Mili, S. Das, K. Nandakumar and R. Lobo, *J. Ethnopharmacol.*, 2021, **281**, 114503.
12 S. Jnaneshwari, M. Hemshekhar, R. M. Thushara, M. Sundaram, M. Santhosh, K. Sunitha, R. L. Shankar, K. Kemparaju and K. S. Girish, *Anti Cancer Agents Med. Chem.*, 2014, **14**, 975–983.
13 N. S. Aparna, S. S. Aswani, M. S. Mohan, P. T. Boban and S. Kamalamma, *Pharmacological Research - Modern Chinese Medicine*, 2023, **9**, 100302.
14 N. R. Prasad, T. Mahesh, V. P. Menon, R. Jeevanram and K. V. Pugalendi, *Environ. Toxicol. Pharmacol.*, 2005, **20**, 1–5.
15 A. F. Majdalawieh, S. H. Ahari, S. M. Yousef and G. K. Nasrallah, *Eur. J. Pharmacol.*, 2023, **960**, 176163.
16 L. Vennila and K. V. Pugalendi, *Redox Rep.*, 2010, **15**, 36–42.
17 I. C. Palheta, L. R. Ferreira, J. K. L. Vale, O. P. P. Silva, A. M. Herculano, K. R. H. M. Oliveira, A. M. J. C. Neto, J. M. Campos, C. B. R. Santos and R. S. Borges, *Molecules*, 2020, **25**, 3300.
18 R. Joshi, M. S. Kumar, K. Satyamoorthy, M. K. Unnikrisnan and T. Mukherjee, *J. Agric. Food Chem.*, 2005, **53**, 2696–2703.
19 T. Geetha, N. Singh, P. K. Deol and I. P. Kaur, *RSC Adv.*, 2015, **5**, 4083–4091.
20 N. Singh, N. Khullar, V. Kakkar and I. P. Kaur, *Environ. Toxicol.*, 2016, **31**, 520–532.
21 M. del Carmen Cruz and J. Tamariz, *Tetrahedron Lett.*, 2004, **45**, 2377–2380.
22 R. G. Wilde, E. M. Welch, J. J. Takasugi, N. G. Almstead, S. M. Rubenstein and H. Beckmann, Acetylamino benzoic acid compounds and their use for nonsense suppression and the treatment of disease, *US Pat.*, 20060167263A1, 2006.
23 A. Mili, S. Birangal, J. Giridhar, K. Nandakumar and R. Lobo, *BMC Chem.*, 2024, **18**, 241.
24 R. A. Friesner, J. L. Banks, R. B. Murphy, T. A. Halgren, J. J. Klicic, D. T. Mainz, M. P. Repasky, E. H. Knoll, M. Shelley, J. K. Perry, D. E. Shaw, P. Francis and P. S. Shenkin, *J. Med. Chem.*, 2004, **47**, 1739–1749.
25 E. Kellenberger, J. Rodrigo, P. Muller and D. Rognan, *Proteins:Struct., Funct., Genet.*, 2004, **57**, 225–242.
26 M. Kontoyianni, L. M. McClellan and G. S. Sokol, *J. Med. Chem.*, 2004, **47**, 558–565.
27 C. R. W. Guimarães and M. Cardozo, *J. Chem. Inf. Model.*, 2008, **48**, 958–970.
28 K. J. Bowers, E. Chow, H. Xu, R. O. Dror, M. P. Eastwood, B. A. Gregersen, J. L. Klepeis, I. Kolossvary, M. A. Moraes and F. D. Sacerdoti, in *Proceedings of the 2006 ACM/IEEE Conference on Supercomputing*, 2006, pp. 84–es.
29 R. G. Wilde, E. M. Welch, J. J. Takasugi, N. G. Almstead, S. M. Rubenstein and H. Beckmann, Use of acetylamino benzoic acid compounds for nonsense suppression and the treatment of disease, *US Pat.*, 7763656B2, 2010.
30 F. Abu, C. N. Mat Taib, M. A. Mohd Moklas and S. Mohd Akhir, *Evid. base Compl. Alternative Med.*, 2017, 2907219.
31 E. Orellana and A. Kasinski, *Bio-Protoc.*, 2016, **6**, 1–7.
32 OECD, *OECD Guidel. Test. Chem.*, DOI: 10.1787/9789264071049-en.
33 A. E. Giri, V. Rao, S. Singhal, K. Gourishetti, S. Biswas, K. Nandakumar, M. R. Chamllamudi, J. Dave, R. Dave, S. Sumalatha and N. Kumar, *Indian J. Pharm. Educ. Res.*, 2020, **54**, 1080–1088.
34 R. F. Beers and I. W. Sizer, *J. Biol. Chem.*, 1952, **195**, 133–140.
35 H. P. Misra and I. Fridovich, *J. Biol. Chem.*, 1972, **247**, 3170–3175.
36 M.-L. Hu, *Methods Enzymol.*, 1994, **233**, 380–385.
37 D. E. Paglia and W. N. Valentine, *J. Lab. Clin. Med.*, 1967, **70**, 158–169.
38 A. W. T. Konings and E. B. Drijver, *Radiat. Res.*, 1979, **80**, 494–501.